Thermal decomposition of ammonium nitrate on rust surface: Risk of low-temperature fire

Ibukun Oluwoye [a], Sara Mosallanejad [a], Goruck Soubans [a], Mohammednoor Altarawneh [b], Jeff Gore [c], Bogdan Z. Dlugogorski [d,*]

[a] *Murdoch University, Discipline of Chemistry and Physics, College of Science, Health, Engineering and Education, 90 South Street, Murdoch, WA, 6150, Australia*
[b] *United Arab Emirates University, Chemical and Petroleum Engineering Department, Sheikh Khalifa bin Zayed St, Al-Ain, 15551, United Arab Emirates*
[c] *Dyno Nobel Asia Pacific Pty Ltd, Mt Thorley, NSW, 2330, Australia*
[d] *Charles Darwin University, Energy and Resources Institute, Ellengowan Drive, Darwin, NT, 0909, Australia*

ABSTRACT

Ammonium nitrate (AN, NH_4NO_3) remains classified as an oxidising agent for transport, storage and handling purposes. The safe use of ammonium nitrate requires strict procedures as AN is incompatible with many materials. This study investigates the thermal decomposition of AN on surfaces of rust, potentially present on steel in storage facilities of AN. Infrared spectroscopy and X-ray diffraction served to characterise the mineralogy of the rust, relatively to neat iron (III) oxide. Furthermore, simultaneous thermogravimetric measurements and differential scanning calorimetry afforded the isoconversional analysis that yields the activation energies of the decomposition process. The results, in conjunction with the molecular modelling involving oxygen-deficient Fe_2O_3 clusters, elucidate the effect of rusts, existing on the surface of corroded steel, in reducing the ignition temperature of AN. This process manifests itself by lowering the activation energies of the initiation channels of the decomposition reactions. On the contrary, pure Fe_2O_3 does not influence the decomposition of AN. The dehydroxylation of hydrated iron (III) oxide, present on surfaces of rust, exposes the Fe sites that react exothermically with AN, before the material assumes the ordered Fe_2O_3 phase.

1. Introduction

Ammonium nitrate (AN, NH_4NO_3) constitutes the primary ingredient of fertilisers and civilian explosives. It is widely deployed as an oxidiser in propulsive engines, gas generator systems (e.g., in automotive inflator systems and heavy-lift launchers) and emergency starters because of its positive oxygen balance, as well as relatively low cost, chemical stability, halogen-free combustion products, and low sensitivity to friction and impact [1–7]. While some scientific interest lies in eliminating the technical drawbacks of AN applications, considerable bodies of research work continually focus on improving the safe operational logistics (i.e., storage and handling) of this hazardous material.

Oxley and co-workers [8] provided a timely account of some accidents (i.e., unintended fires and explosions) pertaining to AN and its composite mixtures. The report shows that, even in the absence of organic materials, AN sometimes ignites at temperatures as low as 95 °C by hot surfaces, leading to thermal runaway, fires or explosions, depending on the level of confinement. For instance, in Belgium

(Tessenderloo, 1942) an AN pile of about 200 tonnes exploded as a result of "caking" and ignition by a disaggregating tool in the presence of impurity [8,]. A similar incident occurred in the United States (West Virginia, 1966) due to hot steel [8]. Examples of recent accidents include that of a fertiliser plant in the United States (Texas, 2013) [10], and a loaded truck in Australia (Wyandra, Queensland, 2014) [11]. These kind of uncontrolled fires of AN have secondary consequences; they result in the formation of nitrogen oxides (NO_x) which contributes to atmospheric pollution [1,12]. In addition to N_2, the decomposition chemistry of AN produces other nitrogen species such as NO_x, and N_2O, via ionic and radical mechanisms in the condensed medium [13,14] and the gas phase [15,16,46].

Due to the incompatibilities of AN with various materials (summarised in Table 1), the US National Fire Protection Association recommends storing the chemical away from acid, alkaline, reducing and combustible materials in a cool, dry and well-ventilated environment [17]. Moreover, the preferred shipping and storage materials are steel and aluminium structures, expected to be non-reactive in the

Table 1

Selected incompatibility of AN with some chemicals [23].

Substances	Effects on AN
Powdered metals	Most metals react violently or explosively with fused ammonium nitrate below 200 °C. Metals may also sensitise AN to shock. They are sometimes referred to as monometallic catalysts.
Metal oxides	Metal oxides lower the ignition temperature of AN-fuel mixtures.
Metal sulfides	Metal sulfides induce the runaway reactions, resulting in detonation at temperatures below 40 °C, if the pH is less than 2.
Metal nitrite/nitrate	Magnesium nitrate may desensitise AN. Contact of AN with potassium nitrite causes incandescence.
Urea	Dehydrated AN in mixtures containing 35–39% urea can produce a residue capable of deflagration at 240 °C. The recommended processing temperature for such formulation should not exceed 120 °C.
Ammonia	Free ammonia may either stabilise or destabilise the AN salt depending on the condition.
Halide salts	Halide salts promote the thermal decomposition of AN, and lower the initiation temperature sufficiently to give a violent or explosive decomposition, i.e., premature spontaneous ignition.
Acids	Mineral acids destabilise AN. Concentrated acetic-acid mixtures ignite AN on warming.
Organic fuels	Organic fuels increase the heat of combustion. Between 2 and 4% of organic fuel are used in commercial explosives.

non-powdered form [17,18]. Metal surfaces often exhibit oxide layers. Under the ambient condition, species of iron oxides and hydroxide, typically known as rust, form on steel surfaces. As shown in Table 1, metal sulfides induce premature detonation of AN, a common phenomenon in mine sites (termed as reactive ground) containing iron pyrite (iron sulfide, FeS_2). Table 1 shows that, metal oxides affect the ignition behaviour of both AN and AN-fuel mixtures. However, the role of complex oxide-hydroxide compounds like rust may be different.

Recent studies focusing on enhancing the performance and physicochemical properties of AN have demonstrated that, some transition metal oxides such as MO_x (M = manganese, cobalt, nickel and copper) influence the endothermic decomposition of AN [19]. Nanoparticles of titanium dioxide (TiO_2) and copper oxide (CuO) enhance the decomposition of AN by decreasing the overall activation energy of the process [20–22]. These oxides, when shaped as nanorods, provide Lewis acid and/or active metal sites, enabling the elimination of NH_3, an intermediate species that usually inhibits the decomposition of AN.

Rust represents a complex mixture of different phases of iron (III) oxide (Fe_2O_3) and its hydrated forms, arising as the product of redox reaction of iron and oxygen in the presence of ambient moisture on steel surfaces. Therefore, rust can easily form on the covers of steel drums and containers filled with AN. This work investigates the influence of rust, constituting the surface of corroded steel, on low-temperature decomposition of commercially-sourced AN. We applied thermal analysis techniques, reinforced by surface reaction modelling, to examine the interaction mechanism of rust particles and AN, quantifying the chemical process by employing the isoconversional kinetic approach. We make relevant comments on fire safety during the storage, transportation and handling of ammonium nitrate.

2. Materials and methods

2.1. Preparation and characterisation of warehouse rust

We scraped rust particles off the corroded surface of mild steel (i.e., a type of carbon steel with low carbon content, between 0.05 and 0.25 mass %), employing them for further analysis as is, i.e., without any treatment. The particle size of the acetone-dispersed rust sample amounted to <20 μm, as determined by optical microscopy. We digested the rust in aqua regia solution, followed by analysis in the inductively coupled plasma - optical emission spectrometry (ICP-OES) to confirm 70% Fe, 0.4% Mn, 0.05% Ti, 0.04% Cr, 0.08% As and 0.08% Ni. The collected material comprised typical chemical species present on iron

surfaces in any industrial setting, including warehouses. Vibrational spectroscopy, performed on Agilent Cary 670 Fourier transform infrared (FTIR) spectrometer equipped with an attenuated-total-reflectance (ATR) sampling accessory, produced the IR spectra of the rust powder (1 mg). The spectrometer operated at a spectral resolution of 4 cm^{-1}, averaging 32 accumulated scans per spectrum on a deuterated lanthanum-alanine doped triglycine sulphate (DLaTGS) detector. Fig. 1 depicts the IR spectra of the rust particles as compared to pure Fe_2O_3. The IR spectrum of the steel rust highlights a broad O–H vibration depicting the presence of hydrated (and hydroxylated) phases of iron oxide. In agreement with the previous observation of Veneranda et al. [24], the ATR sampling methodology is less sensitive to surface O–H species on the rust sample. The broad O–H signal of the rust indicates that, the IR absorptions of this bond occur at varying frequencies due to a range of different chemical interactions at the vicinity of the bonds.

We conducted the phase characterisation of the rust using the X-ray powder diffraction (PXRD) on an GBC eMMA instrument. Our PXRD method involved the scanning angle (2θ) range of 5°–70°, at a regular step size of 0.010° and speed of 1°/min, using a Ni filtered Cu Kα$_1$ radiation (λ = 1.5406 Å). The voltage and current were set to 35 mV and 28 mA, respectively. Match! 3 software processed the acquired spectra by comparing them with the reference patterns from the Crystallography Open Database (COD). The diffractogram in Fig. 2 qualitatively indicates that, the rust sample contains mainly Fe_2O_3, Fe_3O_4, and various phases of iron (III) oxide-hydroxide (FeOOH). Previous studies [25–29] confirm the existence of these iron-oxide phases in rust, with FeOOH (lepidocrocite, goethite, and akaganeite) assuming 85.2–100% of the total composition in urban to severe marine conditions [30,31]. The Fe_3O_4 and Fe_2O_3 represent minor components of rust, as reflected in subtle peaks of Fe_2O_3 vibrations (around 500 cm^{-1}, Fig. 1) in the rust sample.

2.2. Thermal analyses

Simultaneous thermal analyses performed on a Netzsch STA 449 F3 Jupiter instrument served to study the thermochemical behaviour of the desiccated samples upon heating. The method employed approximately 10 mg of AN (Sigma-Aldrich, ≥ 99.5%) or mixtures (AN/rust or AN/Fe_2O_3 at 50/50 mass %), placed in an alumina crucible, and heated from 25 °C to 500 °C at the rates of 5, 10, 15 and 20 °C/min. The 50/50 mass % of the mixtures arbitrarily represents a localised contact between AN and rusted surface of steel. The continuous flow rate of the argon amounted to 60 mL/min, as measured under the standard temperature and pressure (STP). Blank runs, completed under identical conditions to the production runs, yielded the thermal-buoyancy and baseline (for heat flow) corrections. All results represent the average mass loss (%) of
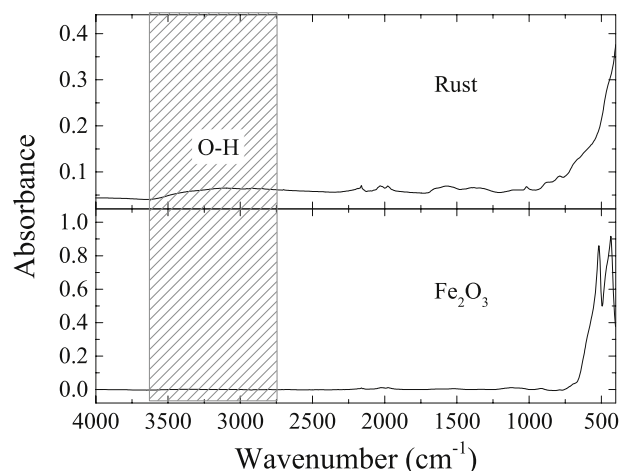
Fig. 1. IR spectra of steel rust and Fe_2O_3.
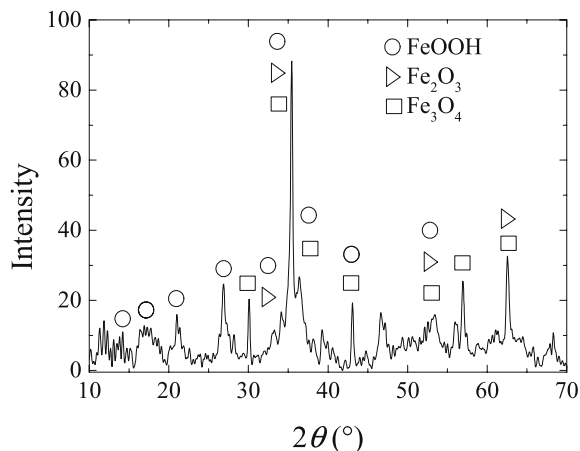
Fig. 2. Particle XRD spectrum of steel rust. The symbols represent the presence of the phases in the sample.

three repeat experiments.

3. Results

3.1. Thermochemical conversion

Fig. 3 depicts the thermal decomposition profile of AN-rust mixture. To confirm the effect of rust on AN decomposition, we ran seperate TGA experiments on the rust and neat AN, calculating the expected physical change in mass (i.e., provided that, no interaction occurs between AN and rust) according to Eq. (1), where $\eta_{expected}$ represents the expected mass loss, with η_{rust} and η_{AN} symbolising the respective mass losses during decomposition of pure rust and AN.

$$\eta_{expected} = (\omega \times \eta_{rust}) + (1 - \omega) \times \eta_{AN} \qquad (1)$$

The TGA curve of rust (Fig. 3b) reveals two distinct steps. The initial mass loss occurring from 30 to 200 °C indicates the dehydration (i.e., elimination of physically adsorbed water) of the rust sample, while the second step between 200 and 350 °C relates to the hydroxylation (destruction of the hydroxyl groups; $2FeO(OH) \rightarrow Fe_2O_3 + H_2O$) of iron (III) hydroxy-oxide [25]. A previous experimental study provides detailed information of the dehydroxylation mechanism of various polymorphs of FeOOH, concluding that, the thermal desorption of OH produces bare Fe surface sites (i.e., OH vacancies), before the final relaxation into Fe_2O_3 [32].

As shown in Fig. 3a, the trend of "AN + rust$_{expected}$", constructed from the expected mass loss $\eta_{expected}$ in Eq. (1), resembles that of pure AN and AN-Fe_2O_3. Whereas, the actual AN-rust (see spectrum for AN + rust in Fig. 3a) decomposition expounds the thermal interaction between AN and rust. The result shows that, rust (from the surface of mild steel) decreases the decomposition temperature of AN. For instance, the extrapolated onset temperature decreases from ca. 250 °C–225 °C in the presence of rust. Such effect does not transpire on the theoretically estimated (based on the individual mass loss of AN and rust) profile and that of AN + Fe_2O_3 (<5 μm). The enhanced decomposition effect of rust, as opposed to Fe_2O_3, can be attributed to the concurrent dehydroxylation of FeOOH. The dehydroxylation step yields an active intermediate comprising the Fe sites that catalyse the decomposition of AN.

Furthermore, the DSC traces in Fig. 4 elucidate how rust particles switch the endothermic decomposition of pure AN (or AN + Fe_2O_3) into a highly exothermic process. Both cases sustain the usual phase changes prior to decomposition, following the sequence IV → II → I → melt, at 52

(a)

(b)

(c)
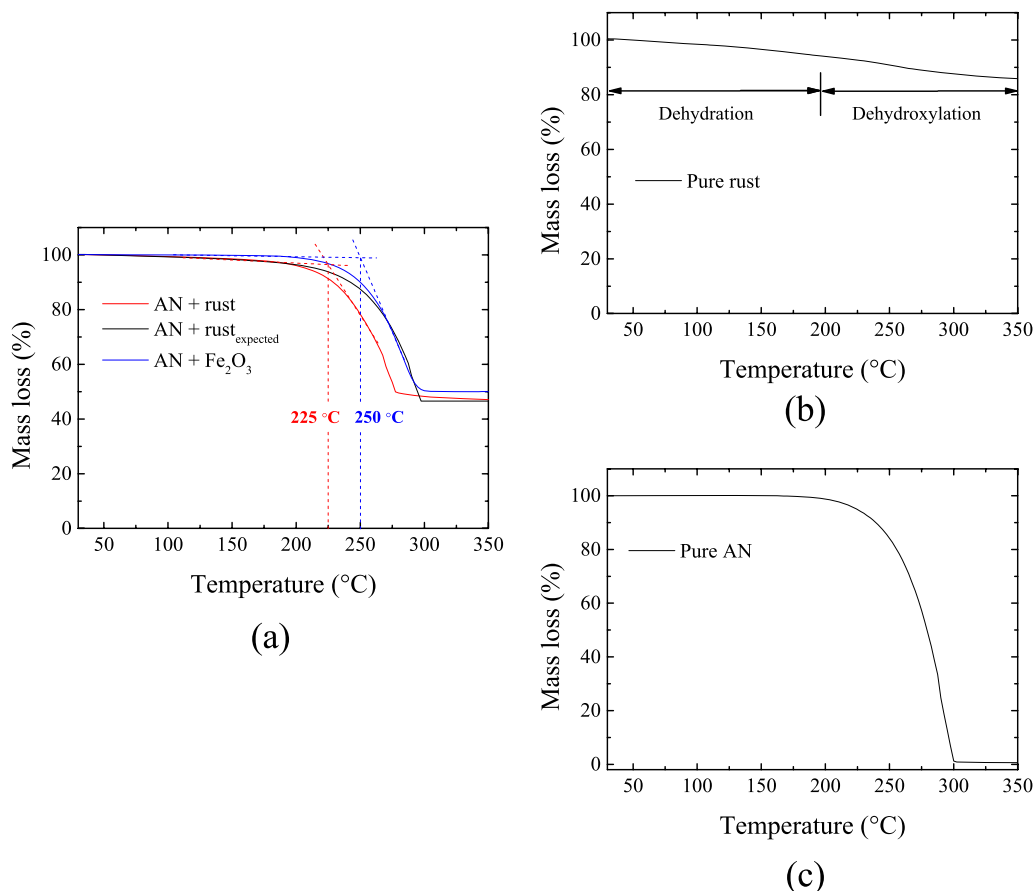
Fig. 3. TGA profiles of the AN-rust mixture as compared to the expected (and AN-Fe_2O_3 mixture) plots. Heating rate equals 20 °C/min.
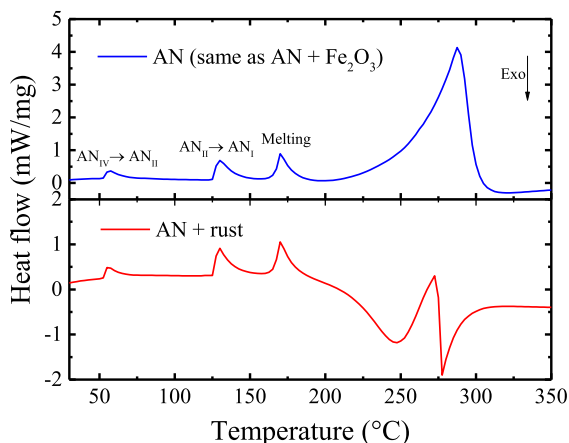
Fig. 4. DSC profiles of the AN-rust mixture as compared to AN (or AN-Fe$_2$O$_3$ mixture). Heating rate corresponds to 20 °C/min.

Fig. 5. Activation energies of thermal decomposition AN and AN-rust mixture. The accuracy thresholds (i.e., error bars) fall inside the size of the marker symbols.

°C, 126 °C and 169 °C, respectively [33,34].

An accidental explosion of AN may manifest itself in two forms; firstly, due to shock waves from primary high explosives (primers), and secondly, as a result of a self-sustaining fire in a confined space [1]. Fig. 4 reinforces the latter, indicating that rust can catalyse and sustain fires (i.e., deflagrations) of AN, which may transition into an explosion (i.e., detonation). Therefore, steel drums, vessels and wall-liners in AN facilities should be inspected for rusts to alleviate the fire risks, especially for AN stored near hot-surfaces or localised energy sources.

3.2. Kinetic analysis

The advanced isoconversional method of Vyazovkin [35,36] enabled an accurate estimation of activation energies for the thermal decomposition process as a function of the conversion α. The term α refers to the fractional conversion of solid sample (i.e., AN or blends) into gaseous products, and it represents the normalised form of mass loss data from the thermogravimetric analysis, in terms of initial mass before the thermal analysis m_i, instantaneous mass at any temperature m_t, and the final mass after the entire decomposition process m_f, according to Eq. (2).

$$\alpha = \frac{m_i - m_t}{m_i - m_f} \qquad (2)$$

Our previous study provides a detailed application of such method [37]. Briefly, for a series of runs performed at different heating rates, the activation energy (E_α, with the subscript α signifying the conversion) corresponds to a value that minimises the objective function in Eq. (3), with the integer subscripts i and j representing different experiments performed under varying heating programs, and $I(E,T)$ signifying the Arrhenius temperature integral.

$$\varnothing(E_\alpha) = \sum_{i=1}^{n} \sum_{j \neq i}^{n} \frac{I(E_\alpha,\ T_{\alpha,i})\beta_j}{I(E_\alpha,\ T_{\alpha,j})\beta_i} \qquad (3)$$

As shown in Fig. 5, the E_α-dependence of pure AN amounts to 92 ± 4 kJ/mol, indicating a single-step decomposition in agreement with the previously reported range of 84–98 kJ/mol [38,39]. The presence of rust (mainly FeOOH) enhances the ignitability of AN by decreasing the activation energies at the early stage of the decomposition process. Evidently, rust surfaces of mild steel induce facile decomposition of AN. We expect such effect to be proportionate to the relative ratio of rust in the blend. The subsequent activation energies (as α increases) exceed that of pure AN as a consequence of simultaneous dehydroxylation events as well as heterogeneous interactions of decomposition products of AN with the iron oxide. Naya and Makoto [40] have investigated the
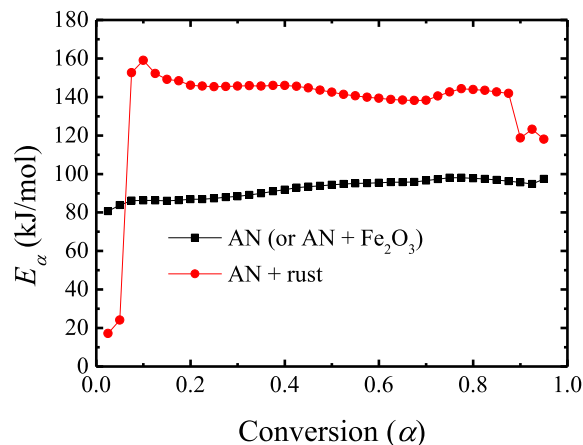
effect of Fe$_2$O$_3$ as a catalyst on the decomposition of ammonium nitrate-based composite propellants using the thermogravimetric - differential thermal analyser in a flow of inert nitrogen gas. The authors demonstrated that, the addition of pure Fe$_2$O$_3$ does not decrease the activation energy values of the decomposition of AN. Apparently, Fe$_2$O$_3$ occurs as a basic oxide and cannot absorb NH$_3$, the Lewis base intermediate species that usually inhibits the decomposition of AN.

3.3. Atomistic reaction mechanism

DMol^3 code afforded all structural optimisations and energy calculations. We implemented the generalised gradient approximation (GGA) of the Perdew-Burke-Ernzerhof (PBE) functional [41,42]. The treatment of electronic cores comprised all-electron relativistic effects and deployed a double numerical plus polarisation (DNP) basis set. The total energy achieved a tolerance of 1×10^{-6} Ha and the calculated energies were adjusted via a dispersion correction term based on the Tkatchenko and Scheffler approach (i.e., a van der Waals DFT-D functional) [43]. We considered thermal smearing of 0.005 Ha and a global cut-off of 4.3 Å in all computations. Convergence tolerance for energy change, maximum force and maximum displacement between the optimisation cycles were set at 0.00002 Ha, 0.004 Ha/Å and 0.005 Å, respectively. Finally, we located the transition states by a complete LST/QST method, and calculated all energy values at 0 K.

We employed a nanocluster of iron oxide-hydroxide (FeOOH)$_{n=8}$, built from the bulk structure of goethite (α-FeOOH) [44], to represent the Fe-exposed intermediate structure of rust. The optimised structure of the nanocluster comprises three- and four-fold coordinated oxygen and iron atoms, in that order. In addition, all Fe–O bonds are electronically equivalent. The calculated Fe–O bond lengths in the nanocluster fall between 1.80/1.95 Å. The concurrent dehydroxylation of FeOOH leads to the enhanced decomposition of AN; see the description of the TGA experiments. In other words, the FeOOH should be activated (i.e., begin to be dehydroxylated) to influence the decomposition of AN. Therefore, we imposed a hydroxyl vacancy on the cluster by deleting one of the OH groups coordinated with iron. This process simulates the occurrence of Fe site characterised by a dangling bond. Similar to the mechanism of low-temperature desulfurisation (i.e., removal of H$_2$S) over the FeOOH [45], the exposed Fe sites can interact with the initial decomposition products of AN.

Gas-phase decomposition of AN is known to begin with an endothermic dissociation step, as depicted in Eq. (4), followed by decomposition of HNO$_3$ and subsequent oxidation of NH$_3$ according to Eq. (5)–(8), respectively [1].

I. Oluwoye et al.

$$NH_4NO_3 \rightarrow NH_3 + HNO_3 \tag{4}$$

$$HNO_3 + HX \rightarrow NO_2^+ + H_2O + X^- \tag{5}$$
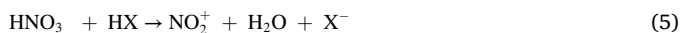
where $HX = NH_4^+$, HNO_3, H_3O^+, and others

$$NH_3 + NO_2^+ \rightarrow \text{products } (N_2O, H_2O) \tag{6}$$

$$NH_3 + X^- \rightarrow \text{products } (NO, NO_2, H_2O) \tag{7}$$

$$HNO_3 \rightarrow OH + NO_2 \tag{8}$$
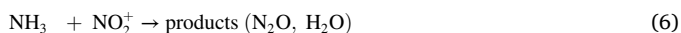
As illustrated in Fig. 6, the presence of species of activated (i.e., Fe exposed) iron oxide-hydroxide catalyse, by highly exothermic absorption, the initiation step of destroying NH_3, a gas molecule that ordinarily retards the decomposition of AN.

4. Conclusions

This study has described the effect of steel rust in increasing the risk of fire of ammonium nitrate. Corroded mild steel, present in a typical warehouse, exhibits layers of hydrated and hydroxylated forms of iron (III) oxide on its surface. Unlike the neat Fe_2O_3, the rust species increase the ignition characteristics of AN, by lowering the activation energy of the initial decomposition steps to as little as 20 kJ/mol. The most plausible reaction mechanism involves the surface destruction of NH_3, an intermediate species that usually inhibits the decomposition of AN, via Lewis acid and/or metal sites on the activated facets of iron-oxide particles. Such effects translate into a reduction in the onset decomposition temperature of AN, as well as highly exothermic decomposition of ammonium nitrate. Therefore, facilities conventionally relying on steel containers for AN storage and transportation should develop protocols to identify and promptly remove any rust forming on container surfaces to avoid possible fires or explosions of AN.

Declaration of competing interest

The authors declare that they have no known competing financial interests or personal relationships that could have appeared to influence the work reported in this paper.
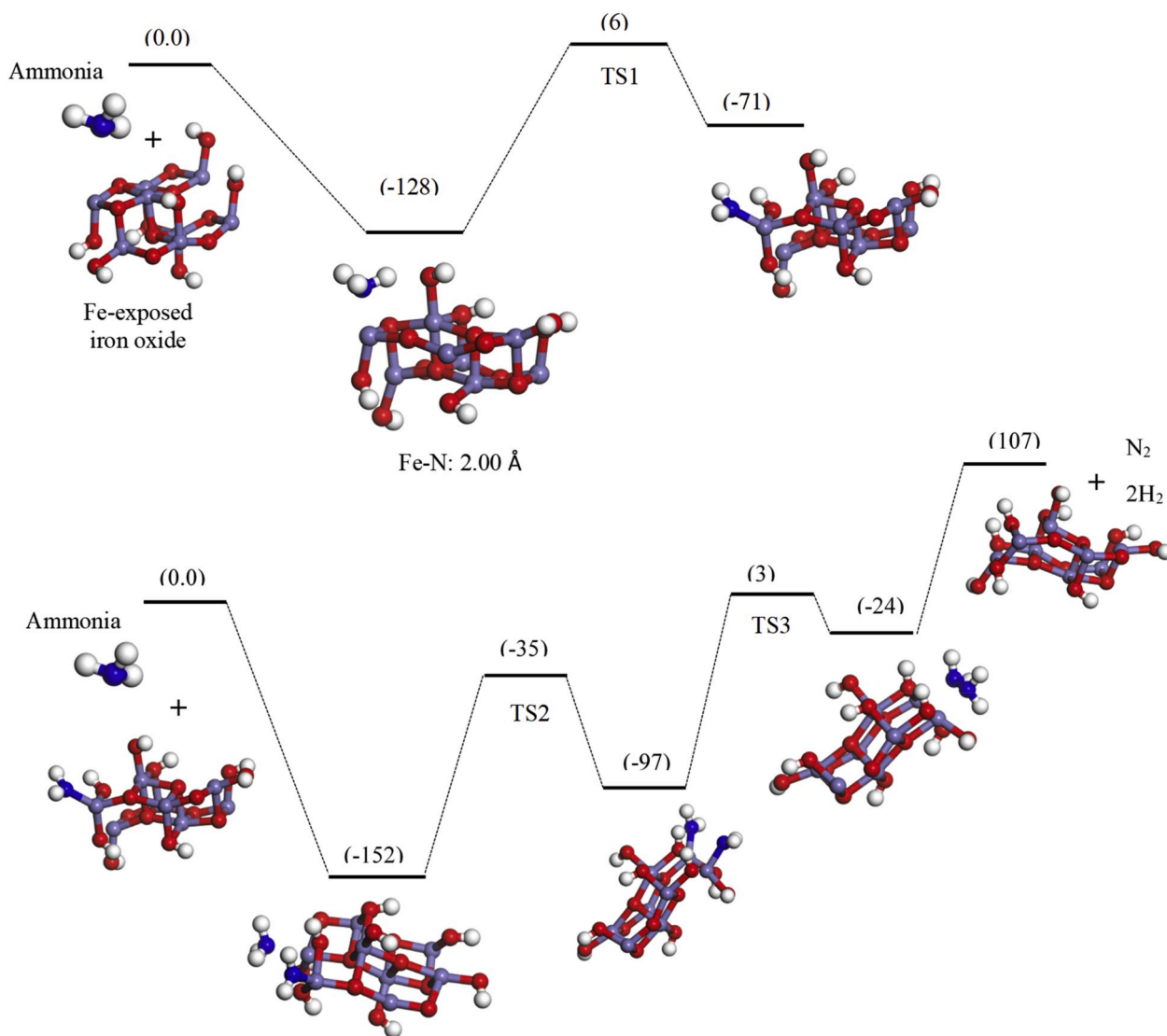
Fig. 6. Mechanism of heterogeneous interaction of NH_3 molecule with activated iron oxide-hydroxide. The white, blue, red and grey represent hydrogen, nitrogen, oxygen and iron, respectively. Energy values are reported in kJ/mol with respect to the initial reactants at 0 K. Note that one hydrogen molecule, remains adsorbed on the surface increasing potential hazards of the reaction(For interpretation of the references to colour in this figure legend, the reader is referred to the Web version of this article.)

References

[1] I. Oluwoye, B.Z. Dlugogorski, J. Gore, H.C. Oskierski, M. Altarawneh, Atmospheric emission of NO_x from mining explosives: a critical review, Atmos. Environ. 167 (2017) 81–96.

[2] J. Jos, S. Mathew, Ammonium nitrate as an eco–friendly oxidizer for composite solid propellants: promises and challenges, Crit. Rev. Solid State Mater. Sci. 42 (2017) 470–498.

[3] A. Ulas, G.A. Risha, K.K. Kuo, Ballistic properties and burning behaviour of an ammonium perchlorate/guanidine nitrate/sodium nitrate airbag solid propellant, Fuel 85 (2006) 1979–1986.

[4] Y.-D. Seo, S.H. Chung, J.J. Yoh, Automotive airbag inflator analysis using the measured properties of modern propellants, Fuel 90 (2011) 1395–1401.

[5] A. Grinberg Dana, G. Tvil, L. Winter, G.E. Shter, G.S. Grader, Pressure effect on the combustion of aqueous urea ammonium nitrate alternative fuel, Fuel 159 (2015) 500–507.

[6] B. Mosevitzky, G.E. Shter, G.S. Grader, Effect of equivalence ratio on the thermal autoignition of aqueous ammonia ammonium nitrate monofuel, Combust. Flame 188 (2018) 142–149.

[7] C. Oommen, S.R. Jain, Ammonium nitrate: a promising rocket propellant oxidizer, J. Hazard Mater. 67 (1999) 253–281.

[8] J.C. Oxley, J.L. Smith, E. Rogers, M. Yu, Ammonium nitrate: thermal stability and explosivity modifiers, Thermochim. Acta 384 (2002) 23–45.

[10] West Fertilizer Co, Failed to Disclose it Had Unsafe Stores of Explosive Substance, Huffington Post, April 20, 2013.

[11] C. Atfield, Truck Explosion Injures Eight, Closes Mitchell Highway, Brisbane Times, September 6, 2014.

[12] J.P. Agrawal, High Energy Materials: Propellants, Explosives and Pyrotechnics, Wiley-VCH, Weinheim, 2010.

[13] Y.-i. Izato, A. Miyake, Thermal decomposition mechanism of ammonium nitrate and potassium chloride mixtures, J. Therm. Anal. Calorim. 121 (2015) 287–294.

[14] S.A. Skarlis, A. Nicolle, D. Berthout, P. Dujardin, P. Granger, Combined experimental and kinetic modeling approaches of ammonium nitrate thermal decomposition, Thermochim. Acta 584 (2014) 58–66.

[15] R. Musin, M. Lin, Novel bimolecular reactions between NH_3 and HNO_3 in the gas phase, J. Phys. Chem. A 102 (1998) 1808–1814.

[16] J. Park, M. Lin, Thermal decomposition of gaseous ammonium nitrate at low pressure: kinetic modeling of product formation and heterogeneous decomposition of nitric acid, J. Phys. Chem. A 113 (2009) 13556–13561.

[17] NFPA, Fire Protection Guide to Hazardous Materials, twelfth ed., National Fire Protection Association, Quincy, 1997.

[18] Storage Requirements for Security Sensitive Ammonium Nitrate (SSAN), in: Explosives Information Bulletin No. 53, Queensland Government, Depratment of Natural Resources, Mines and Energy, 2017.

[19] D. Trache, T.M. Klapötke, L. Maiz, M. Abd-Elghany, L.T. DeLuca, Recent advances in new oxidizers for solid rocket propulsion, Green Chem. 19 (2017) 4711–4736.

[20] A.A. Vargeese, K. Muralidharan, Anatase–brookite mixed phase nano TiO_2 catalyzed homolytic decomposition of ammonium nitrate, J. Hazard Mater. 192 (2011) 1314–1320.

[21] A.A. Vargeese, K. Muralidharan, Kinetics and mechanism of hydrothermally prepared copper oxide nanorod catalyzed decomposition of ammonium nitrate, Appl. Catal. Gen. 447–448 (2012) 171–177.

[22] A.A. Vargeese, K. Muralidharan, V.N. Krishnamurthy, Kinetics of nano titanium dioxide catalyzed thermal decomposition of ammonium nitrate and ammonium nitrate-based composite solid propellant, Propellants, Explos. Pyrotech. 40 (2015) 260–266.

[23] L. Bretherick, P. Urben, M.J. Pitt, L. Battle, Bretherick's Handbook of Reactive Chemical Hazards, vol. 1, Butterworth-Heinemann, 1999.

[24] M. Veneranda, J. Aramendia, L. Bellot-Gurlet, P. Colomban, K. Castro, J. M. Madariaga, FTIR spectroscopic semi-quantification of iron phases: a new method to evaluate the protection ability index (PAI) of archaeological artefacts corrosion systems, Corrosion Sci. 133 (2018) 68–77.

[25] Y. Zhao, H. Ren, H. Dai, W. Jin, Composition and expansion coefficient of rust based on X-ray diffraction and thermal analysis, Corrosion Sci. 53 (2011) 1646–1658.

[26] H. Cano, D. Neff, M. Morcillo, P. Dillmann, I. Diaz, D. de la Fuente, Characterization of corrosion products formed on Ni 2.4 wt%–Cu 0.5 wt%–Cr 0.5 wt% weathering steel exposed in marine atmospheres, Corrosion Sci. 87 (2014) 438–451.

[27] S.J. Oh, D. Cook, H. Townsend, Characterization of iron oxides commonly formed as corrosion products on steel, Hyperfine Interact. 112 (1998) 59–66.

[28] D. De la Fuente, J. Alcántara, B. Chico, I. Díaz, J. Jiménez, M. Morcillo, Characterisation of rust surfaces formed on mild steel exposed to marine atmospheres using XRD and SEM/Micro-Raman techniques, Corrosion Sci. 110 (2016) 253–264.

[29] T. Kamimura, S. Nasu, T. Tazaki, K. Kuzushita, S. Morimoto, Mössbauer spectroscopic study of rust formed on a weathering steel and a mild steel exposed for a long term in an industrial environment, Mater. Trans. 43 (2002) 694–703.

[30] E. Almeida, M. Morcillo, B. Rosales, M. Marrocos, Atmospheric corrosion of mild steel. Part I–Rural and urban atmospheres, Mater. Corros. 51 (2000) 859–864.

[31] D. De la Fuente, I. Díaz, J. Simancas, B. Chico, M. Morcillo, Long-term atmospheric corrosion of mild steel, Corrosion Sci. 53 (2011) 604–617.

[32] X. Song, J.-F.o. Boily, Surface and bulk thermal dehydroxylation of FeOOH polymorphs, J. Phys. Chem. A 120 (2016) 6249–6257.

[33] M.J. Herrmann, W. Engel, Phase transitions and lattice dynamics of ammonium nitrate, Propellants, Explos. Pyrotech. 22 (1997) 143–147.

[34] C.N.R. Rao, M. Natarajan, B. Prakash, S. United, Crystal Structure Transformations in Inorganic Nitrites, Nitrates, and Carbonates, National Bureau of Standards, Washington, 1975.

[35] S. Vyazovkin, Advanced isoconversional method, J. Therm. Anal. 49 (1997) 1493–1499.

[36] S. Vyazovkin, A.K. Burnham, J.M. Criado, L.A. Pérez-Maqueda, C. Popescu, N. Sbirrazzuoli, ICTAC Kinetics Committee recommendations for performing kinetic computations on thermal analysis data, Thermochim. Acta 520 (2011) 1–19.

[37] I. Oluwoye, B.Z. Dlugogorski, J. Gore, S. Vyazovkin, O. Boyron, M. Altarawneh, Thermal reduction of NO_x with recycled plastics, Environ. Sci. Technol. 51 (2017) 7714–7722.

[38] S. Vyazovkin, J.S. Clawson, C.A. Wight, Thermal dissociation kinetics of solid and liquid ammonium nitrate, Chem. Mater. 13 (2001) 960–966.

[39] T. Liavitskaya, N. Guigo, N. Sbirrazzuoli, S. Vyazovkin, Further insights into the kinetics of thermal decomposition during continuous cooling, Phys. Chem. Chem. Phys. 19 (2017) 18836–18844.

[40] T. Naya, M. Kohga, Burning characteristics of ammonium nitrate-based composite propellants supplemented with Fe_2O_3, Propellants, Explos. Pyrotech. 38 (2013) 547–554.

[41] B. Delley, From molecules to solids with the DMol^3 approach, J. Chem. Phys. 113 (2000) 7756–7764.

[42] J.P. Perdew, K. Burke, M. Ernzerhof, Generalized gradient approximation made simple, Phys. Rev. Lett. 77 (1996) 3865–3868.

[43] A. Tkatchenko, M. Scheffler, Accurate molecular van der Waals interactions from ground-state electron density and free-atom reference data, Phys. Rev. Lett. 102 (2009), 073005.

[44] S. Sasaki, Radial distribution of electron density in magnetite, Fe3O4, Acta Crystallogr. Sect. B Struct. Sci. 53 (1997) 762–766.

[45] L. Shen, Y. Cao, Z. Du, W. Zhao, K. Lin, L. Jiang, Illuminate the active sites of γ-FeOOH for low-temperature desulfurization, Appl. Surf. Sci. 425 (2017) 212–219.

[46] I Oluwoye, M Altarawneh, J Gore, B.Z Dlugogorski, Burning properties of redox crystals of ammonium nitrate and saccharides, Combust. Flame 213 (2020) 132–139.